Hexavalent iridium oxide for proton-exchange membrane water electrolysis

The production of hydrogen via electrolysis ($2H_2O \rightarrow 2H_2 + O_2$), powered by renewable energy resources such as solar and wind, is pivotal in the global effort to achieve carbon neutrality by 2050. Among the available technologies, proton-exchange membrane water electrolysis (PEMWE) is advantageous because of its high energy efficiency, rapid on-off response, and low hydrogen crossover, making it an ideal match for the intermittent nature of renewable energy sources. However, a critical barrier to large-scale PEMWE deployment is the reliance on iridium, a rare and expensive metal, as the anode catalyst for the oxygen evolution reaction (OER). The global annual production of iridium is limited to only 7–8 tons, leading to an unsustainable iridium supply for scaling up hydrogen production to meet future demands [1-5]. Addressing this challenge is essential to unlock the full potential of PEMWE in driving the hydrogen economy.

Our research addresses this challenge by developing novel atomically dispersed hexavalent iridium oxide (Ir^{VI}-*ado*) on manganese dioxide (MnO_2) [1]. This catalyst reduces iridium usage by over 95% compared to conventional catalysts while maintaining high catalytic activity and stability. This work not only makes green hydrogen production more cost-effective, but also accelerates the global transition to a sustainable hydrogen economy.

The synthesis of Ir^{VI}-*ado* involves an oxidative ligand-substitution reaction using potassium hexachloroiridate (K_2IrCl_6) and manganese dioxide (MnO_2) as reactants. Comprehensive structural and chemical characterizations were performed using *in situ* and *ex situ* techniques at SPring-8 **BL14B2** (XAFS), **BL39XU** (HERFD-XANES), **BL36XU** (HERFD-XANES), **BL17SU** (XPS and XAFS), and **BL44B2** (SR-PXRD). XAS at the Ir L_3-edge was used to monitor changes in the oxidation state and coordination environment during synthesis, whereas XPS was used to determine the binding energy and oxidation state of Ir in the final catalyst. High-angle annular dark-field scanning transmission electron microscopy (HAADF-STEM) was used to visualize the atomic dispersion of Ir on the MnO_2 support. The electrochemical performance of Ir^{VI}-*ado* was evaluated using a PEM electrolyzer. Additionally, *in situ* XAS was performed to assess the stability of Ir^{VI}-*ado* under operational conditions with current density up to 2 $A \cdot cm^{-2}$.

Successful synthesis of Ir^{VI}-*ado* was achieved by leveraging the oxidative potential of MnO_2, which facilitated the transformation of Ir^{IV} into Ir^{VI}. The XAS spectra showed a shift in the white-line (WL) position of the Ir L_3-edge, reflecting the transition of Ir from the +4 oxidation state in K_2IrCl_6 to a higher oxidation state in the Ir^{VI}-*ado* catalyst during the synthesis process (Fig. 1(a)). The EXAFS results indicated that the Cl ligand in the precursor K_2IrCl_6 was substituted by oxygen in MnO_2, forming Ir–O and Ir–O–Mn coordinations (Fig. 1(b)). The WL intensity, proportional

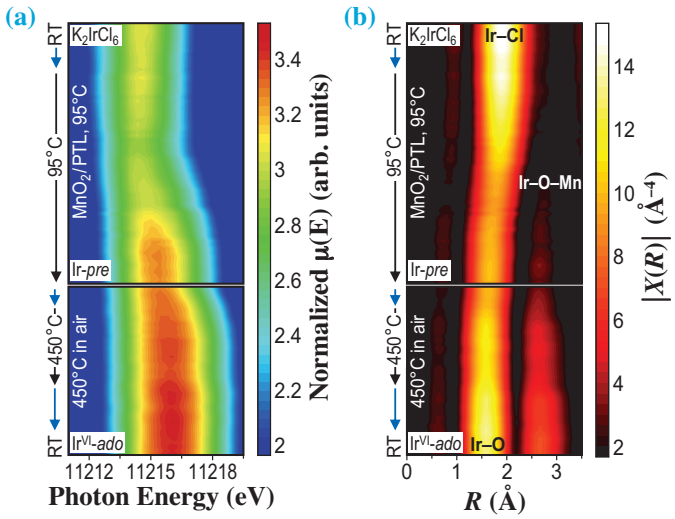

Fig. 1. *In situ* XAS analysis of Ir^{VI} formation. Two-dimensional color maps showing the shift of the absorption edge **(a)** and the coordination shell **(b)** at the iridium L_3-edge peak as a function of time during the synthesis of Ir^{VI}-*ado*. Simplified temperature profiles for heating and cooling (blue arrows) and constant temperature (black arrows) are shown on the left. RT, room temperature.

to the population of 5*d* holes in the iridium atom, indicated an average oxidation state of +5.8 ± 0.1 for Ir^{VI}-*ado* (Fig. 2(a)). Consistently, XPS confirmed that over 80% of the Ir in Ir^{VI}-*ado* existed in the oxidation state of +6, as evidenced by its characteristic binding energy of 62.61 eV for the Ir $4f_{7/2}$ peak. The average Ir–O bond length in Ir^{VI}-*ado* (1.959 Å) was shorter than that in rutile IrO_2 (1.986). *In situ* XAS measurements confirmed that the Ir^{VI} oxidation state was maintained even at high current densities (2.3 A·cm^{-2}) and elevated temperatures (80°C). Scanning electron microscopy (SEM) revealed that the obtained Ir^{VI}-*ado* uniformly covered the porous transport layer (PTL) substrate (Fig. 2(b)). Atomic-resolution HAADF-STEM images showed that Ir was atomically dispersed on the MnO_2 support (Figs. 2(c-e)).

The Ir^{VI}-*ado* catalyst demonstrates remarkable mass-specific activity and stability during the OER under acidic conditions. At an iridium loading of 0.08 mg_{Ir}·cm^{-2}, Ir^{VI}-*ado* achieved a current density of 4.0 A·cm^{-2} at 2 V in a PEM electrolyzer. Long-term stability tests showed minimal degradation over 2700 h operation at 1.8 A·cm^{-2}, highlighting the durability of Ir^{VI}-*ado* under industrial PEMWE operation. Turnover numbers of up to 1.5×10^8 were recorded, which were higher than those of previously reported Ir-based catalysts (Fig. 2(f)). Its ability to maintain high activity and stability under industrial conditions demonstrates the practical viability of Ir^{VI}-*ado* for large-scale hydrogen production. Furthermore, the atomically dispersed nature of Ir enhances its utilization efficiency, enabling >95% reduction in Ir loading compared to that of conventional catalysts. By reducing the Ir requirement to 0.08 mg_{Ir}·cm^{-2}, the annual global production of Ir could support the deployment of over 300 GW of PEMWE capacity per year, representing a significant step toward meeting the 2000 GW target required for carbon neutrality.

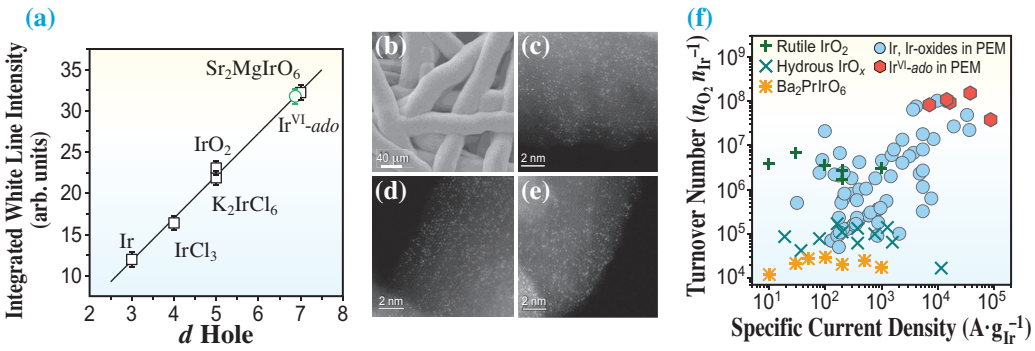

Fig. 2. Characterization of Ir^{VI}-*ado*. **(a)** High-energy resolution fluorescence detected X-ray absorption near edge structure (HERFD-XANES) spectra at the Ir L_3-edge of Ir^{VI}-*ado* and the reference samples. (**b**) SEM image of Ir^{VI}-*ado* fabricated on MnO_2/PTL. Scale bar, 40 μm. (**c** to **e**) HAADF-STEM images of Ir^{VI}-*ado* taken from different sample locations. Iridium atoms (bright dots) are embedded in the surface of MnO_2. Scale bars, 2 nm. (**f**) Turnover numbers plotted *versus* mass-specific current densities for Ir^{VI}-*ado* (I to V; red hexagons) and Ir-based electrocatalysts reported in the literature.

Ailong Li*, Shuang Kong and Ryuhei Nakamura

Biofunctional Catalyst Research Team,
RIKEN Center for Sustainable Resource Science/Wako

*Email: ailong.li@riken.jp

References

[1] *A. Li, S. Kong, K. Adachi, H. Ooka, K. Fushimi, Q. Jiang, H. Ofuchi, S. Hamamoto, M. Oura, K. Higashi, T. Kaneko, T. Uruga, N. Kawamura, D. Hashizume and R. Nakamura: Science* ***384*** *(2024) 666.*
[2] A. Li *et al.*: Angew. Chem. Int. Ed. **58** (2019) 5054.
[3] A. Li *et al.*: Nat. Catal. **5** (2022) 109.
[4] S. Kong *et al.*: Nat. Catal. **7** (2024) 252.
[5] A. Li *et al.*: Innov. Mater. **2** (2024) 100094.